Human Molecular Genetics, 2003, Vol. 12, No. 17 2109–2120
DOI: 10.1093/hmg/ddg189

A mouse model for cystinuria type I

T. Peters†, C. Thaete†, S. Wolf, A. Popp, R. Sedlmeier, J. Grosse*, M.C. Nehls, A. Russ and V. Schlueter

Ingenium Pharmaceuticals AG, Fraunhoferstr. 13, 82152 Martinsried, Germany

Received March 31, 2003; Revised and Accepted May 24, 2003

Cystinuria, one of the most common inborn errors of metabolism in humans, accounts for 1–2% of all cases of renal lithiasis. It is caused by defects in the heterodimeric transporter system rBAT/b$^{0,+}$AT, which lead to reduced reabsorption of cystine and dibasic amino acids through the epithelial cells of the renal tubules and the intestine. In an *N*-ethyl-*N*-nitrosourea mutagenesis screen for recessive mutations we identified a mutant mouse with elevated concentrations of lysine, arginine and ornithine in urine, displaying the clinical syndrome of urolithiasis and its complications. Positional cloning of the causative mutation identified a missense mutation in the solute carrier family 3 member 1 gene (*Slc3a1*) leading to an amino acid exchange D140G in the extracellular domain of the rBAT protein. The mouse model mimics the aetiology and clinical manifestations of human cystinuria type I, and is suitable for the study of its pathophysiology as well as the evaluation of therapeutic and metaphylactic approaches.

Downloaded from http://hmg.oxfordjournals.org/ by guest on January 13, 2014

INTRODUCTION

With an estimated prevalence of 1 in 7000 (1), cystinuria is one of the most common inborn errors of metabolism in humans. Cystinuria is predominantly inherited as an autosomal recessive trait, and is caused by defective transport of cystine and dibasic amino acids (lysine, arginine and ornithine) through the epithelial cells of the renal tubules and the intestinal brush border, resulting in elevated urine concentrations of these amino acids. Impaired reabsorption of poorly soluble cystine from primary urine leads to a high risk for the formation of cystine calculi in the urinary tract, potentially causing obstruction, infections and eventually renal failure.

Clinically, this syndrome is either classified as type I or non-type I cystinuria. Both types are distinguished on the basis of the cystine and dibasic aminoaciduria of the obligate heterozygotes (1). The type I form is fully recessive and displays a normal urinary cystine excretion pattern in heterozygous individuals, whereas non-type I forms are incompletely recessive and show moderate to high hyperexcretion of cystine and dibasic amino acids in heterozygous patients (1). The treatment of cystinuria is directed at reducing the cystine concentration by different approaches. Dietary restrictions to reduce cystine production and excretion and attempts to increase cystine solubility by increased fluid uptake are commonly used. Additionally, patients are treated with drugs like D-penicillamine, mercaptopropionylglycine or Captopril (1), which enhance cystine solubility. Frequently, interventions like lithotripsy are required.

Following the identification of rodent cDNAs encoding cystine transporters (2,3), mutations in the human *SLC3A1* gene were identified in 1993 as the major molecular defect underlying type I cystinuria (4–6). *SLC3A1* encodes the protein rBAT, the heavy subunit of the heterodimeric rBAT-b$^{0,+}$AT amino acid transporter system in intestinal and renal epithelial cells. This heterodimeric sodium-independent transporter is responsible for the uptake of cystine and dibasic amino acids from food in the intestine and from ultrafiltrate in the renal tubules.

rBAT is a type II membrane glycoprotein with a short intracellular N-terminal domain, followed by a single transmembrane helix and a large extracellular domain (7,8). To build the functional transporter system b$^{0,+}$, rBAT forms a heterodimer with the protein b$^{0,+}$AT encoded by *SLC7A9* (9). Both proteins are linked through a covalent disulfide bond. So far a number of mutations in *SLC3A1* associated with the completely recessive cystinuria type I have been described in humans whereas mutations in *SLC7A9* mainly cause non-type I but occasionally also cystinuria type I (10–13). Hence, a novel genotypic classification scheme has recently been proposed reclassifying cystinuria in type A (*SLC3A1* mutations) and type B (*SLC7A9* mutations) (10).

Several animal models but no murine model for cystinuria have been identified (reviewed in 1). Cystinuria in dogs was already described in 1823 and is up to now the best

*To whom correspondence should be addressed. Tel: +49 8985652392; Fax: +49 8985652351; Email: johannes.grosse@ingenium-ag.com
†The authors wish it to be known that, in their opinion, the first two authors should be regarded as joint First Authors.

 © Oxford University Press 2003; all rights reserved

characterized and most widely used model for studying the disease. For Newfoundland dogs, cystinuria could be attributed to a mutation within the *SLC3A1* gene (14).

Here we describe the first murine model for type I cystinuria, caused by an *N*-ethyl-*N*-nitrosourea (ENU)-induced mutation in *Slc3a1* resulting in a single amino acid substitution in the extracellular domain of rBAT.

RESULTS

Identification of an uremic mouse line

We performed a genome-wide mutagenesis screen to generate medically relevant phenotypic alterations in the mouse and to identify their causative recessive mutations. Mutations were induced by ENU treatment of C3HeB/FeJ mice, followed by a three-generation breeding scheme to obtain animals homozygous for the induced mutations (15,16). Several hundred families of 15–25 G3 animals, each one derived from a G1 founder animal carrying a unique set of mutations, were phenotyped by a broad set of assays.

In one of these pedigrees, three males were identified with elevated serum levels of urea (131.5 ± 39.3 mg/dl; normal range 20–68 mg/dl), indicating impaired renal function. In addition, alkaline phosphatase (ALP; 182 ± 56 U/l; normal range 90–163 U/l), low-density lipoprotein cholesterol (LDL; 15.5 ± 9.7 mg/dl; normal range 2–9 mg/dl) and total cholesterol (150.7 ± 44.5 mg/dl; normal range 100–180 mg/dl) were elevated.

This phenotype was confirmed with a recessive pattern of inheritance on C3HeB/FeJ inbred background as well as in an outcross/intercross to the MRL/MpJ background. Similar to the founding generation, males were predominantly affected.

Because of the presence of impressive calculi (see below), the mutant mouse line was named *Pebbles* (*pbl*).

Genetic mapping and identification of a mutation in *Slc3a1*

Analysis of 440 meioses (220 individuals) from the C3HeB/FeJ X MRL/MpJ mapping cross identified the *pbl* locus in a region of ~8.3 cM or 7.74 Mb at the distal end of mouse chromosome 17, between markers *D17Mit72* and *D17Mit12* (Fig. 1A).

This candidate region shares a conserved synteny with a genomic segment on human chromosome 2 (2p22.2–22.1), containing the solute carrier family 3 member 1 gene (*SLC3A1*) encoding rBAT, a subunit of the heterodimeric amino acid transporter $b^{0;+}$. Mutations in SLC3A1 cause human cystinuria type I (17), making its mouse ortholog (18) an excellent candidate gene for the observed uremia phenotype.

Like the human gene, mouse Slc3a1 is encoded by 10 exons spanning a genomic region of ~33.6 kb in a region of conserved synteny (Fig. 1D). Nucleotide sequence analysis of Slc3a1 genomic DNA from affected mice revealed an A→G transition at nucleotide position 464 in exon 1 creating a *Stu*I restriction site (Fig. 1B). The conceptual translation of Slc3a1 (464A→G) predicts a missense mutation leading to a substitution of glycine (GGC) for aspartic acid (GAC) at amino acid position 140 located in the extracellular domain of the protein. Amino acid sequence analysis revealed a significant homology of a subregion of the extracellular domain (amino acid residues 124–506) to the α-amylase domain of members of the Glycosyl hydrolase family 13 (8,19,20). Notably, the alignment of the amino acid sequence of the α-amylase-like domain of rBAT vertebrate orthologs demonstrated that D140 is highly conserved, even in related α-amylase domains of members of the glycosyl hydrolase family 13 (Fig. 1C).

The Slc3a1 (464A→G) variant could not be identified in the parental C3HeB/FeJ or other inbred strains, indicating that this mutation was induced by ENU. It strictly co-segregates with the pbl phenotype, suggesting an etiology similar to human cystinuria type I. In the mapping cross the penetrance of the pbl mutation was determined to be 95.6% in males (22/23 of homozygotes) and 6.25% in females (1/16).

Slc3a1 expression is unchanged in mutant animals

To determine the tissue distribution of murine *Slc3a1*, 49 different tissues from wild-type (wt) male and female animals were tested by RT–PCR for *Slc3a1* mRNA expression. Strong expression in both genders was detected in kidney, liver, gall bladder and different parts of the intestine. Weaker expression of *Slc3a1* was found in pancreas, bladder and the medulla oblongata. In males expression was also found in testis. In embryos, expression of *Slc3a1* was detectable from day E9.5 onwards (data not shown).

Northern blot analysis of kidney tissue revealed a transcript pattern with a predominant 2.4 kb transcript similar to the pattern reported previously (18). No differences in the expression level between wild-type, heterozygous and homozygous animals could be detected (data not shown). Likewise, *in situ* hybridization of kidney sections as well as quantitative real-time PCR experiments also showed no differences in *Slc3a1* expression levels between wild-type and homozygous mutant kidney, demonstrating that the mutation does not significantly alter transcript levels (Fig. 2A and B).

Elevated urinary amino acid levels cause urolithiasis

Hexagonal microcalculi indicative for cystine crystals were found in all homozygous animals investigated, including all females (Fig. 3A). In contrast, X-ray analysis and necropsy revealed the presence of calculi in bladder and/or kidney of all homozygous males (9/9) but only two out of seven females (23%) at an age between 8 and 12 months (Fig. 3C and D). This gender preference is also observed in cystinuria of dogs and wolves (1,10). The number and diameter of calculi differed significantly between individuals, with the largest concrements reaching a diameter of 5 mm (Fig. 3B).

Chemical analysis of calculi identified cystine as the only amino acid present (Fig. 4B), confirming the analogy to the cystinuria syndrome in humans.

In urine, both homozygous males and females displayed significantly elevated levels of lysine, arginine and ornithine when compared with their wild-type and heterozygous littermates at an age of 80–150 days (Fig. 4A; ANOVA, *post hoc* Bonferroni test; $P < 0.05$). Urinary amino acid concentrations were elevated 74-fold for arginine, 37-fold for lysine and

Downloaded from http://hmg.oxfordjournals.org/ by guest on January 13, 2014

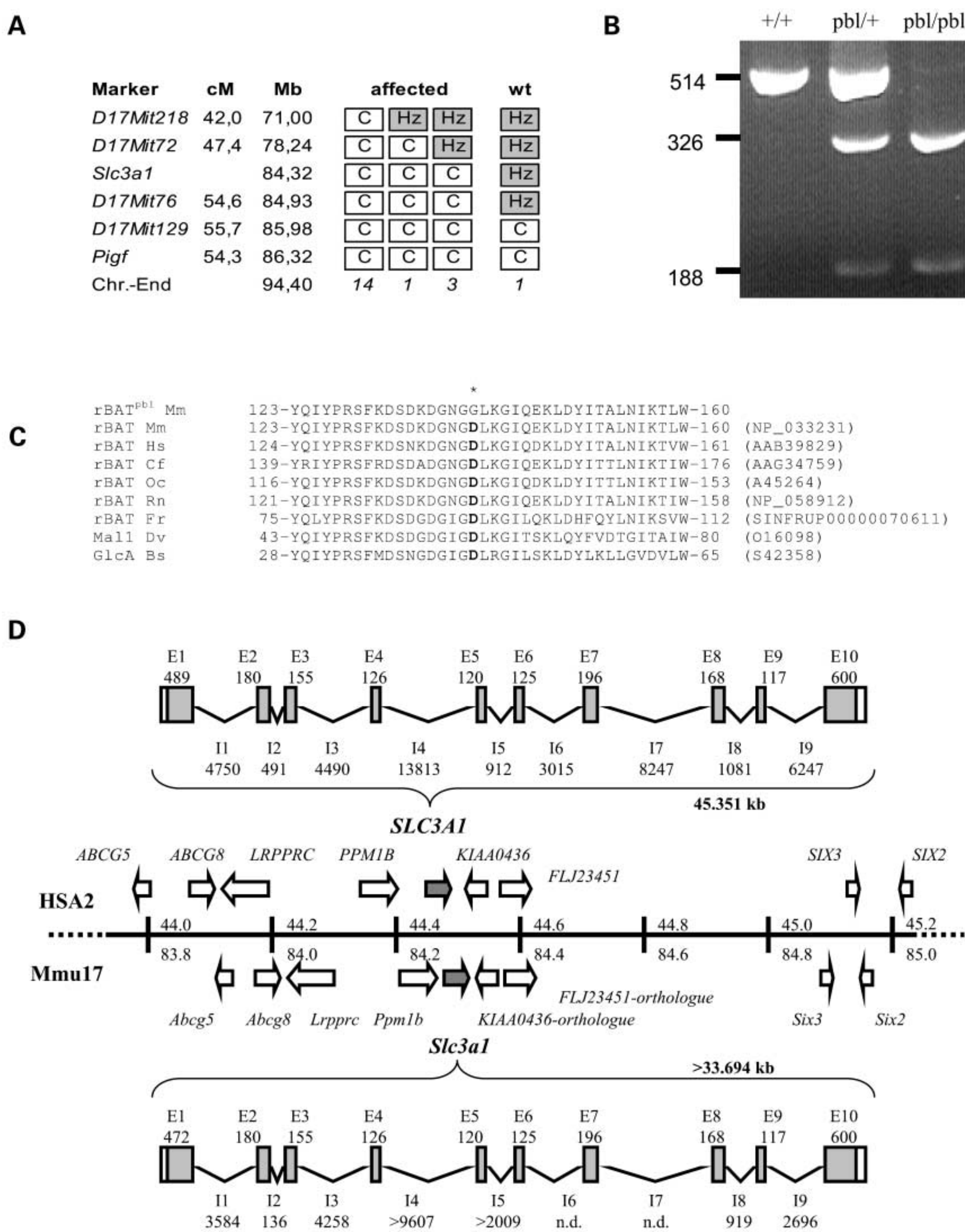

Figure 1. Chromosomal mapping and mutation analysis. (**A**) Haplotype analysis of one non-affected (wt) and 18 affected recombinant male mice, defining the maximal critical interval at the distal end of chromosome 17 containing *Slc3a1*. Genetic (in cM) and physical (in Mb) positions of the analysed loci are given on the left. Haplotypes for each marker are shown as columns with numbers of mice represented beneath. Open boxes indicate homozygosity for C3HeB/FeJ (C) alleles. Shaded boxes denote heterozygosity for C3HeB/FeJ and MRL/MpJ alleles (Hz). (**B**) Restriction fragment-length polymorphism genotyping assay of the specific mutation in *Slc3a1* based on the difference in the *Stu*I restriction pattern between wild-type (514 bp) and mutated nucleic acid sequences (326 and 188 bp products). (**C**) Partial alignment of vertebrate rBAT amino acid sequences and related α-amylase domains of proteins of the glycosyl hydrolase family 13 (Mal1, Maltase I precursor, GlcA, α-glucosidase). The asterisk marks the D140 mutated in *Slc3a1*^{pbl} mice. GenBank accession numbers and Ensembl protein ID (*Fugu rubripes*) are given on the right. Mm, *Mus musculus*; Hs, *Homo sapiens*; Cf, *Canis familiaris*; Oc, *Oryctolagus cuniculus*; Rr, *Rattus norvegicus*; Fr, *F. rubripes*; Dv, *Drosophila virillis*; Bs, *Bacillus.* sp. (**D**) Comparative physical map of HSA2 and Mmu17 and schematic illustration of the genomic structure of human and mouse *Slc3a1*. A 1.2 Mb orthologous region enclosing *SLC3A1* on human chromosome 2 (HSA2, 44.0–45.2 Mb) and mouse chromosome 17 (Mmu17, 83.8–85.0 Mb) is shown (middle panel). Known genes with names above (human genes) or below (mouse genes) are displayed as arrows indicating their direction of transcription. The genomic structure of human and mouse *Slc3a1* is given in the upper and the lower panel, respectively. Filled and open boxes indicate translated and non-translated exons (E1–10), respectively, with size of individual exon (in bp) below. Thin lines indicate introns (I1-9) with size (in bp) below. Genomic data were assembled from the Ensembl and UCSC genome databases (43,44).

Downloaded from http://hmg.oxfordjournals.org/ by guest on January 13, 2014

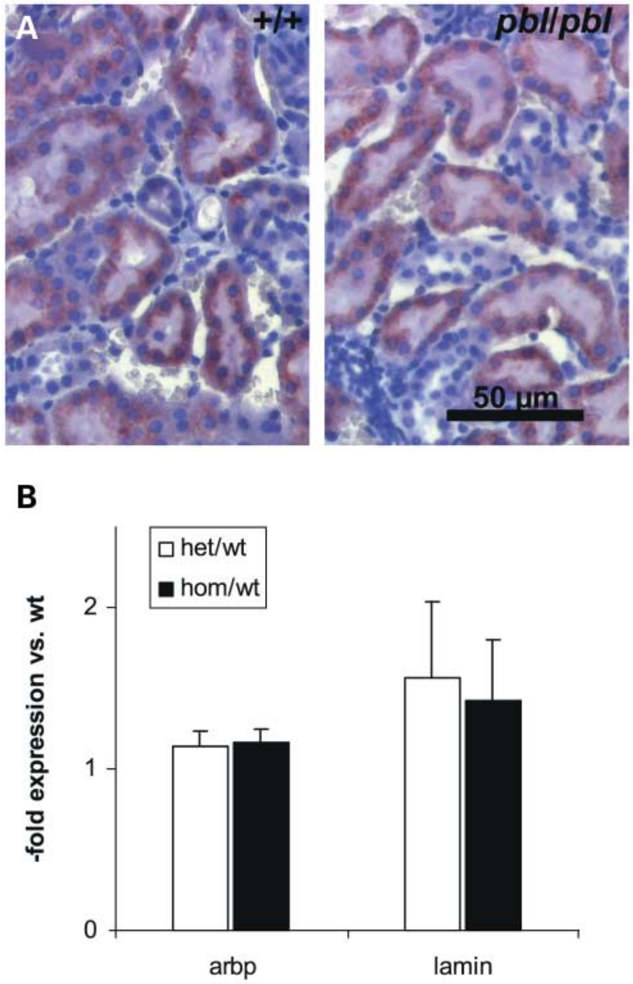

Figure 2. (**A**) *In situ* hybridization analysis of *Slc3a1* expression (brown staining) in epithelial cells of the renal tubules revealed no difference between kidney sections isolated from a wild-type littermate (left) and a mutant *pbl/pbl* female (right) at an age of 8 months. Sections were counterstained with Hoechst 33258 fluorescent dye to show cell nuclei. (**B**) Expression of *Slc3a1* relative to acidic ribosomal phosphoprotein P0 (arbp) or lamin as housekeeper was studied by LightCycler PCR. Normal weighted kidneys of *pbl/pbl* or *pbl/+* mice were compared with wt litter mates. cDNAs of four to six kidneys were pooled and used in two different dilutions. Results of two independent experiments per dilution are represented as mean $\pm$ SD.

6.6-fold for ornithine in females, and 19-fold (arginine), 9.4-fold (lysine) and 3.8-fold (ornithine) in males. In wild-type animals, no gender differences for any of the amino acids was detected (e.g. arginine, wt males 13.8 ± 3.6 µmol/l; wt females 12.5 ± 6.7 µmol/l; *t*-test, $P > 0.05$). The difference in the urinary amino acid concentrations of *pbl/pbl* homozygous males and females was restricted to inbred animals and not observed in the mixed genetic background (data not shown).

Plasma levels of arginine, lysine and ornithine were not different between genotypes (ANOVA, $P > 0.05$), indicating that the mutant animals can compensate completely for the urinary loss of these amino acids. Plasma levels of 15 other amino acids were also unchanged (data not shown).

Not unexpectedly, the levels of cysteine in urine correlated only weakly with the concentrations of the basic amino acids, suggesting that the level of free cysteine is mainly controlled by homodimerization to cystine and the formation of disulfide bonds with proteins.

Urolithiasis is associated with histopathological features of congestion kidney

Necropsy and histopathology revealed the secondary changes typical for urolithiasis. Kidneys were mostly affected unilaterally with organ weights being reduced to between one-half and one-third of the norm (Fig. 5). In kidneys of affected homozygous males, hematoxylin/eosin (H&E) stained sections showed uni- or bilateral dilation of the pelvis and an atrophy of the functional tissue (medulla and cortex, Fig. 6D). To some extent colorless crystalline concrements were visible in the kidney pelvis (Fig. 6C). Renal tubules and glomerula were dilated and contained flocculent, eosinophilic material (Fig. 6B). Tubular epithelia were flattened and capillary loops of most glomerula were compressed. Additionally, the prismatic epithelial layer of the glomerula (male-specific in mice) was flattened and the underlying basal lamina was thickened (Fig. 6B). In individual animals, focal interstitial inflammation and/or basophilic stained tubules (indicative of regenerated tubules) were obvious (Fig. 6B). These pathological changes were observed in at least one kidney of animals presenting with urolithiasis (9/9 males; 2/7 females).

Liver, small and large intestine and pancreas showed no histopathological changes.

The genetic background modulates clinical consequences of the Slc3a1pbl mutation

Uremia was present in all homozygous males in the C3HeB/FeJ background (Fig. 7), with serum creatinine being significantly elevated (wt, 0.064 ± 0.024 mg/dl; heterozygous, 0.078 ± 0.039 mg/dl; homozygous, 0.145 ± 0.054 mg/dl, $n \geq 4$ per genotype; ANOVA, $P < 0.05$; *post hoc* Bonferroni test). Females bearing calculi also consistently showed impaired renal function. As expected, the prevalence of urolithiasis and uremia increased over lifetime, with only one out of 16 females affected at 134 days of age (6.25%), while two out of seven had developed stones at an age of 8–12 months. In C3HeB/FeJ males, significant progression of renal disease was observed between an age of 13 and 19 weeks (Fig. 7).

In the mixed C3HeB/FeJ/MRL/MpJ background, most parameters were significantly elevated at 13 weeks already, without clear progression during the following 6 weeks (Fig. 7). In the C3HeB/FeJ background, body weight of homozygous males was not significantly different from wt or heterozygous animals during the first 3 months of life, while later their body weight was significantly reduced. In the mixed background, a significant reduction of body weight was already observed shortly after weaning. This suggests a modulation of the clinical manifestation by the genetic background, with a later onset and slower progression in C3HeB/FeJ inbred males compared with males of mixed background. Irrespective of the genetic background, females showed a more moderate reduction of body weight, that did not reach statistical significance (Fig. 8A).

Downloaded from http://hmg.oxfordjournals.org/ by guest on January 13, 2014

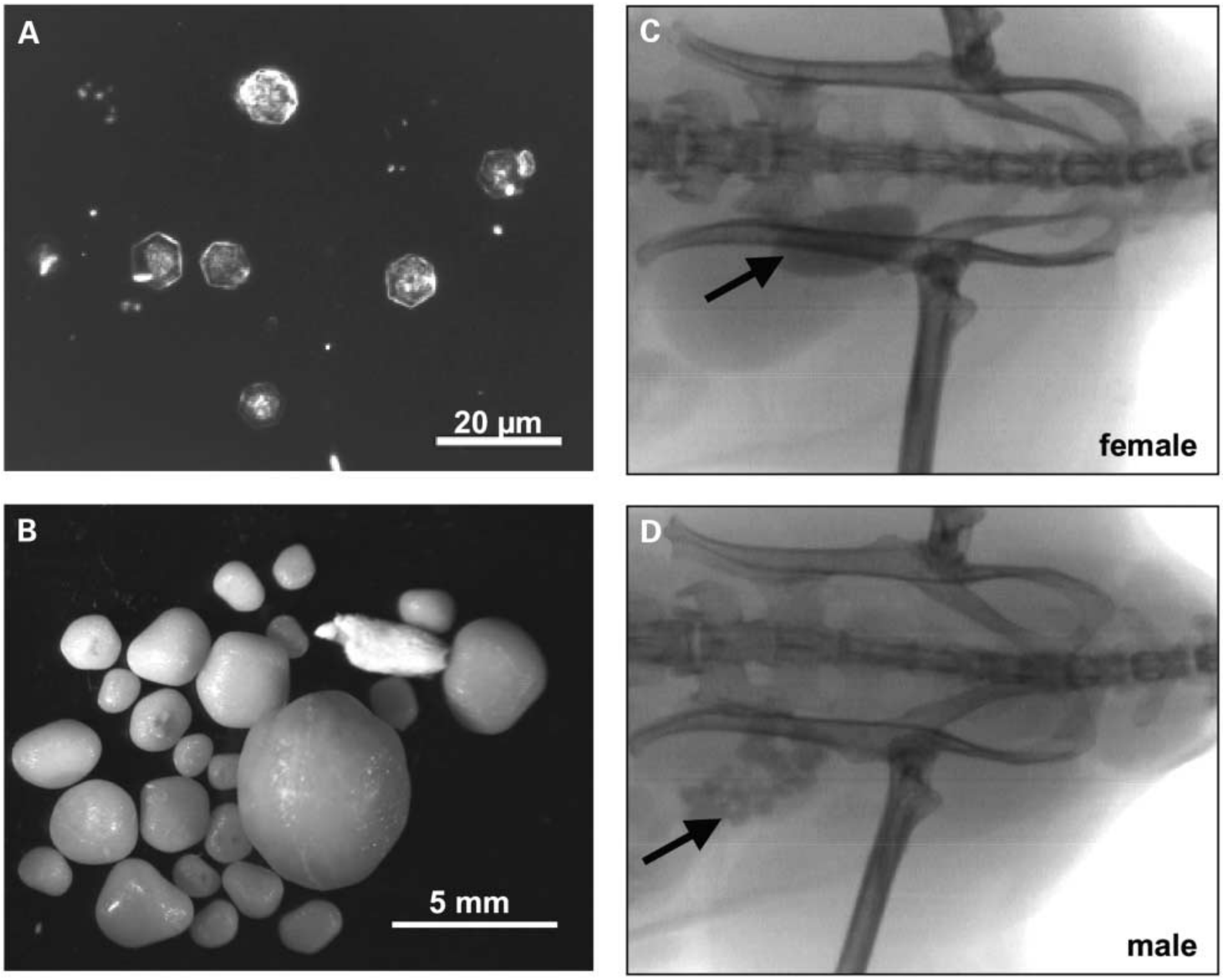

Figure 3. Aspect and localization of cystine calculi. (**A**) Hexagonal microcrystals indicative for cystine calculi found in the urine of homozygous animals. (**B**) Calculi isolated from the bladder of a 7-month-old male homozygous animal. (**C**, **D**) X-ray analysis showed dark, round spots (arrow) in the bladder of homozygous animals. Cystine calculi, which are usually not visible in radiographs, appear as dark areas because of incorporated minerals.

Reduction of body weight is due to a reduction in fat mass

Analysis of body composition by dual-energy X-ray absorption (pDEXA) revealed that lean mass was not altered in males, whereas *pbl/pbl* females showed a moderate but significant increase. Fat mass was significantly reduced in both genders (Fig. 8B). As no uremia was present in the *pbl/pbl* females investigated this observation was unexpected, suggesting that significant alterations in the metabolic steady state take precedence overt uremia.

Bone mineral density was significantly reduced in both *pbl/pbl* males and females. As in the reduction of fat mass, the effect on bone mineral density was more pronounced in males compared with females (Fig. 8B).

DISCUSSION

ENU-induced mutagenesis is an established method to introduce random point mutations throughout the genome (15). Screening for medically relevant phenotypes lead to the identification of the mouse strain *Pebbles* (*pbl*), resembling many features of human cystinuria type I (1), most conspicuously formation of smooth, round and oval cystine calculi in the urinary tract and with high levels of dibasic amino acids in urine. The mutation was mapped to a region of 8 Mb and subsequently detected in the *Slc3a1* gene encoding the rBAT protein, one component of the heterodimeric amino acid transporter $b^{0;+}$ (21).

Most estimates of the mutation load induced by ENU are based on the specific locus test, which relies on phenotypic detection of mutations disrupting the function of a known gene. In an optimized ENU regimen, the average mutation rate is reported to amount to one in 1000 per tester locus (22). Assuming a number of 30 000–35 000 genes in the murine genome, this would mean that each founder animal carries 30–35 recessive mutations, with an average distance of 42–48 cM between two functionally relevant mutations (23). Thus, it is very unlikely that the pbl phenotype is caused by two co-segregating independent mutations, especially if the large

Downloaded from http://hmg.oxfordjournals.org/ by guest on January 13, 2014

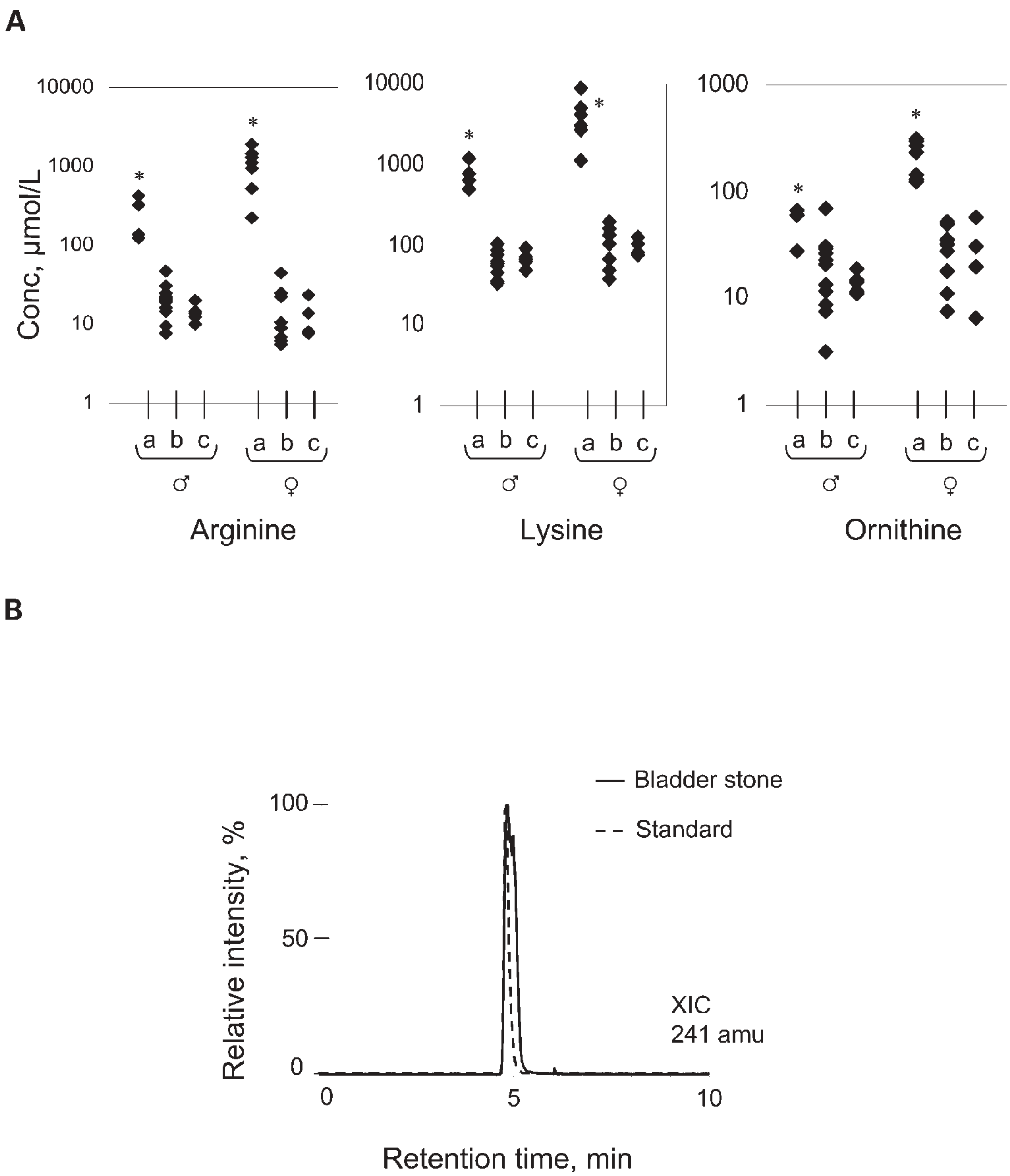

Figure 4. Urine amino acid levels were determined by electrospray tandem mass spectrometry (ESI MS/MS). (**A**) Homozygous male and female animals show a significant increase of lysine, arginine and ornithine (a, *pbl/pbl*; b, *pbl/+*; c, +/+). Significance is indicated by an asterisk; ANOVA, $P = 0.05$, Bonferroni *post hoc* test; $n \geq 4$ per genotype. (**B**) Detection of cystine with cystine standard solution (L-cystine, Sigma C8755) at 241 amu (atomic mass units) of re-dissolved bladder stones from selected homozygous animal.

number of meioses investigated to map the mutation is taken into account.

About 60 different mutations are described for human *SLC3A1*, all of them being linked to cystinuria (17). The mutations are distributed across the entire gene without any predilection sites. Many of them are missense, only a few are nonsense mutations, insertions or deletions. rBAT proteins encoded by human and murine *Slc3a1* contain 685 amino acids and show 78% identity and 86% similarity, respectively. The evolutionary conservation of both genes is also demonstrated by the preservation of the individual gene architecture of orthologous *Slc3a1* genes as indicated by identical exon sizes and a conserved relative spacing of exon sequences within the human and mouse gene.

In our ENU mutagenesis screen we identified a yet undescribed mutation causing a D140G amino acid exchange. The mutation has no detectable effect on the expression of *Slc3a1*mRNA, suggesting that neither transcription nor mRNA

Downloaded from http://hmg.oxfordjournals.org/ by guest on January 13, 2014

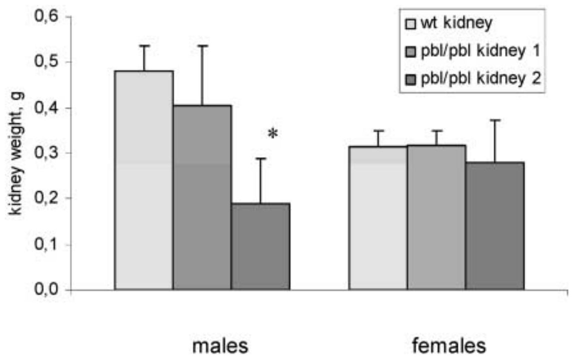

Figure 5. Kidney weight of 8- to 12-month-old homozygous male and female mice was determined. Significance is indicated by an asterisk; *t*-test, $P < 0.05$, $n = 9$ for males; $n = 6$ for females. Male *pbl* homozyotes have a significant reduced weight of one kidney compared with their wild-type littermates, whereas *pbl* homozygous females have not. No difference in kidney weight was seen between wild-type and heterozygous animals (data not shown).

stability is dramatically changed. The mutation might affect protein stability, localization or function.

The extracellular domain of the rBAT protein contains two functional distinguishable domains (reviewed in 8). Deletion studies suggested the most carboxy-terminal part to be involved in the transport process (24,25). The remaining larger part comprising amino acids 125–512 shows significant similarity (46%) to the α-amylase domain (also called central domain of glycosidases) consensus sequence. The core structure of this domain is constituted of alternating α-helices and β-sheets forming an inner barrel of eight β-sheets and an outer barrel of eight α-helices. The functional significance of this structure for rBAT is difficult to infer as this domain occurs in a large variety of proteins performing completely different tasks. The inner barrel is filled with hydrophobic residues, thus excluding the possibility that it forms a part of the translocation pore. The location of the putative catalytic site points away from the cell membrane. It might have a catalytic function or may bind ligands (8).

Functional analysis of the mutations within the α-amylase domain revealed impaired translocation of the rBAT/$b^{0,+}$AT to the cell surface. These trafficking defects are also detectable in mutations of the carboxy-terminal domain, but in addition the transport characteristics of the heterodimeric complex are changed in these mutations (8).

The D140G mutation of the *pbl/pbl* mouse is located at the highly conserved start of the first helix possibly destabilizing the double barrel structure. According to the structural model described above this should result in a trafficking defect without disturbing the transport characteristics of the heterodimeric complex.

Impaired reabsorption of cystine caused by impaired function of rBAT in the proximal tubules of the kidney results in elevated cystine concentrations in urine and due to its poor solubility consequently in the formation of cystine stones. Cystine crystals are assumed to precipitate in the kidney, to accumulate in the bladder and finally grow in both compartments to form calculi with a diameter of up to 5 mm. Urinary tract obstruction leads to hydronephrosis and ultimately to loss of renal parenchyma and uremia.

Similar to other animal models (14), our *Slc3a1*^{pbl} mutant mice showed a delayed onset or, alternatively, a reduced penetrance of stone formation in females. While all *pbl/pbl* males developed urolithiasis during the first year of life, only 23% of *pbl/pbl* females presented with stones at this age. At an age of 4.5 months only one out of 16 females (6.25%) suffered from uremia, suggesting an increased prevalence over the lifetime of the females.

Urine levels of basic amino acids were similar or higher in *pbl/pbl* females than in males. This suggests that the reduced incidence of stone formation might be due to anatomical differences between the male and female urinary system as described previously for Canidae (26,27). Alternatively, metabolic differences in males and females might influence the development of stones. The fact that microcrystalluria was present in all females investigated supports the hypothesis that the initial stages of formation of calculi are similar in both genders, and that progression is slower in females as small crystals are cleared more effectively through the short urethra.

Uremia was correlated with the presence of stones in all cases investigated, and elevated levels of ALP, cholesterol, LDL and the reduction of triglyceride levels have been observed exclusively in association with uremia. Patients with end stage renal disease (ESRD) are reported to have disturbances of the lipid metabolism with elevation of cholesterol, LDL, and triglyceride levels. The causes are a combination of impaired clearance of lipids from the circulation and increased lipid production (28,29). These changes of the lipid metabolism are common risk factors for atherosclerosis and might contribute to the tremendous increase in cardiovascular mortality, although other factors as hormonal and electrolyte alterations and diabetes mellitus are also involved (30,31). These dyslipidemic risk factors for atherosclerosis have not been shown to be risk factors in ESRD patients, and consequently the rationale to correct dyslipidemia has been questioned (32). Another common finding in these patients is the reduced bone mineral density at least in part caused by secondary hyperparathyroidism (33). Parameters of bone turnover increase with declining glomerular filtration rate, thus indicating that alterations in bone metabolism are initiated at early stages of chronic renal failure (34). Recently, a history of kidney stones without overt impairment of kidney function was found to be associated with a reduced bone mineral density in a large epidemiological study (35).

Similar to these observations we found a reduced bone mineral density in *pbl/pbl* females irrespective of the presence or absence of uremia. In addition, *pbl/pbl* mice suffering from kidney stones (i.e. mainly males) had elevated ALP levels which might be related to an increased bone turnover.

In males, the genetic background modified the onset and progression of the renal failure. In C3HeB/FeJ inbred background, plasma parameters as well as body weight were only different from heterozygous and wild-type littermates from 3–4 month of age onwards. In the mixed background (C3HeB/FeJ/MRL/MpJ), body weight was already reduced shortly after weaning, and plasma parameters were abnormal at 3 months of age, with further progression being slower than in inbred mice.

Fat mass was reduced in mutants irrespective of gender and preceded signs of overt uremia in females. The body composition analysis also revealed an apparent increase in

Downloaded from http://hmg.oxfordjournals.org/ by guest on January 13, 2014

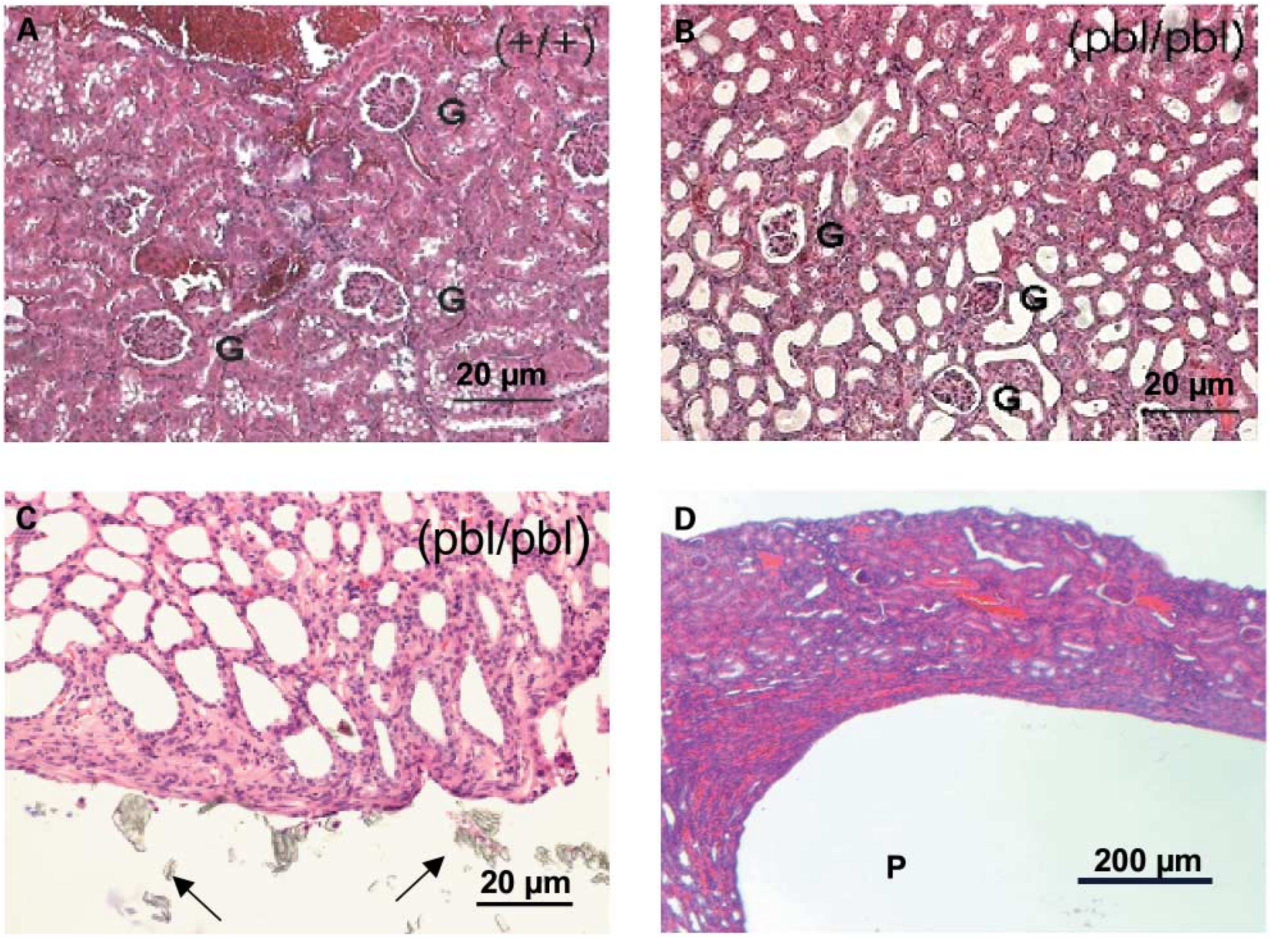

Figure 6. Compared with wild-type (**A**) kidney sections of homozygous (*pbl/pbl*) male mice (**B**) show massive atrophy of functional tissue, dilated tubules and glomerula and flattening of tubular and glomerula epithelia. Capillary loops of most glomerula (G) were compressed. (**C**) Colorless crystals with an orthorhombic prism structure were found in the kidney pelvis of a homozygous animal close to the epithelium (arrow). (**D**) Chronic cystine lithiasis leads to cystic pelvis dilation (P) and atrophy of renal cortex and medulla. H&E staining; magnification as indicated by bar.

lean body mass in *pbl/pbl* females. This intriguing result might be an artifact of the pDEXA analysis. A constant percentage of lean mass is assumed to be water by the lean mass computation algorithm, an assumption possibly leading to an overestimation of lean mass in states of fluid retention. Reductions of apparent lean mass measured by pDEXA before and after hemodialysis have been observed (36–38).

The changes in body composition are probably due to the impaired renal function. This implicates that even in females a subclinical alteration of renal function occurs. In favor of this hypothesis is the observed reduction in bone mineral density, a trend towards reduced body weight not reaching significance in our study and the development of renal insufficiency in some of the females. Alternatively, stones might develop and block the urinary tract temporarily before leaving spontaneously. This inherent painful process and possibly urinary tract infections associated with recurring urolithiasis might induce changes in feeding behavior of the animals.

Protein and energy malnutrition is highly prevalent in patients with chronic renal failure. In ESRD patients a reduction in several nutritional markers including lean mass, bone mineral density and fat mass has been described. The condition improves after onset of chronic hemodialysis (39).

In summary, we describe a first murine model for cystinuria type I. This model might be useful to study the molecular mechanisms involved in the tubular amino acid transport and cystinuria. In addition, clinical consequences of chronic renal failure are observed in the *Pebbles* mouse. Thus, the pathomechanisms of phenomena associated with chronic renal failure irrespective of its origin might be studied in this animal model. Finally, treatments directed at increasing the cystine solubility or at reducing its excretion might be tested in the *pbl/pbl* mouse.

MATERIALS AND METHODS

ENU treatment and breeding

C3HeB/FeJ male mice (The Jackson Laboratory, Bar Harbor, ME, USA) were injected intraperitoneally three times in weekly intervals between 8 and 10 weeks of age with ENU (Serva

Downloaded from http://hmg.oxfordjournals.org/ by guest on January 13, 2014

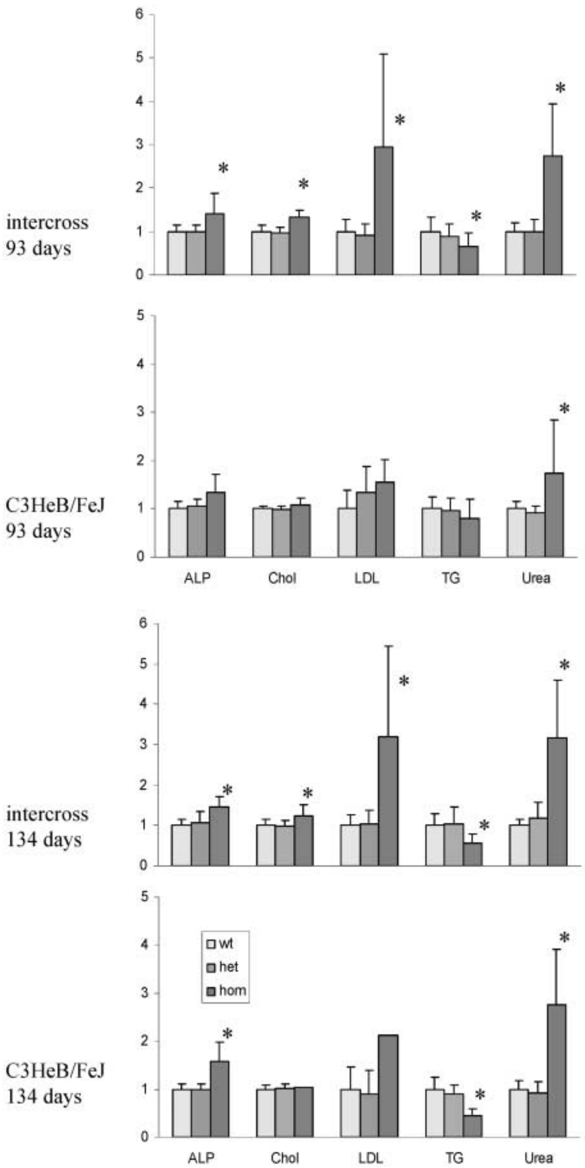

Figure 7. Plasma levels of males of all three genotypes are presented. Males were 93 or 134 days old. The difference caused by the genetic background is clearest at an age of 93 days. At an age of 134 days this difference is largely alleviated. Values are normalized to the wt mean. Error bars represent 1SD. Significance is indicated by an asterisk; ANOVA, $P = 0.05$, Bonferroni *post hoc* test; $n \geq 4$ per genotype and measurement; two values lacking error bars in the lowest panel represent less than four values: only means are presented and measurements were excluded from statistical analysis.

Electrophoresis GmbH, Heidelberg, Germany) at concentrations of 90 mg/kg body weight.

For the recessive screen, unaffected F_1 males were mated with wild-type C3HeB/FeJ females, and G2 offspring were intercrossed to generate G3 animals. One affected animal from this generation was used as the founder of the mutant inbred line.

For genetic mapping, the founder animal was mated with wild-type MRL/MpJ females to generate the F4 animals, which were intercrossed to produce the informative F5 generation. All animals used for breeding were between 8 and 16 weeks of age.

Analysis of blood markers

For phenotypic characterization blood was taken at 93 and again at 134 days of age. Animals starved overnight were bled and blood plasma was separated by centrifugation. Plasma parameters were measured with a Hitachi 912 instrument using the recommended reagents according to the manufacturers instructions (Roche Diagnostics, Mannheim, Germany): calcium, creatinine, phosphate, glutamic-oxaloacetic transaminase (GOT), glutamate pyruvate transaminase (GPT), lactate dehydrogenase, cholinesterase, triglycerides, glucose, total protein, urea, alkaline phosphatase (ALP) cholesterol and low density lipoprotein (LDL).

Reference values for all parameters were determined for wild type inbred and outcross animals. Blood taking and measurements were repeated in suspicious cases.

Chromosomal mapping

For chromosomal mapping of the *pbl* locus homozygous C3HeB/FeJ *pbl/pbl* G3 individuals were outcrossed to MRL/MpJ background. Heterozygous F_4 hybrids were intercrossed and affected F_5 individuals were identified by their characteristic phenotype. A total of 440 meioses were investigated to map the *pbl* mutation. For initial mapping F_5 (C3HeB/FeJ/MRL/MpJ) affected individuals were used. Comparable DNA amounts of eight individuals were pooled and 100 ng pool DNA per PCR reaction was subjected to pool sequencing of 54 single-nucleotide polymorphisms (SNPs) equally distributed over the genome. The content of genomic DNA originating from the C3HeB/FeJ founder strain was interpreted semiquantitatively by visual analysis of individual SNP chromatograms. For this purpose peak altitudes of the pool DNA from affected animals were compared with peak altitudes of the pool DNA from definite C3HeB/FeJ $\times$ MRL/MpJ hybrid animals. High resolution mapping on affected and unaffected (C3HeB/FeJ/MRL/MpJ) intercross animals on an individual basis was carried out by microsatellite analysis with dye-labeled primers (*D17Mit218*, *D17Mit72*, *D17Mit76*, *D17Mit129*) and by SNP sequencing (*Mep1a*, *Pigf*). Microsatellite marker and mapping data were obtained from the Mouse Genome Informatics database (www.informatics.jax.org), the database of the Whitehead Institute for Biomedical Research/MIT Center for Genome Research (www-genome.wi.mit.edu/resources.html) and the Ensembl Mouse v7.3b.2 database update.

Genotyping

To genotype mice for the *Slc3a1* (464A→G) mutation PCR products using primers Slc3a1-3 (5′-ACCAATAACGGGTTTGTCCA-3′) and Slc3a1-4 (5′-GCCTTCAGCAGATAGCCTTG-3′) synthesized from genomic DNA were digested with *Stu*I at 37°C for 4 h and electrophoresed on a 2% agarose gel. After *Stu*I digestion, wild type alleles appear as 514 bp and mutant alleles as 326 and 188 bp products. In addition to the parental C3HeB/FeJ strain and the outcross strain MRL/MpJ the following inbred strains were screened for the *pbl* polymorphism: AKR, BALB, C57BL/6, CAST/EI, DBA, 129J and NZB.

Downloaded from http://hmg.oxfordjournals.org/ by guest on January 13, 2014

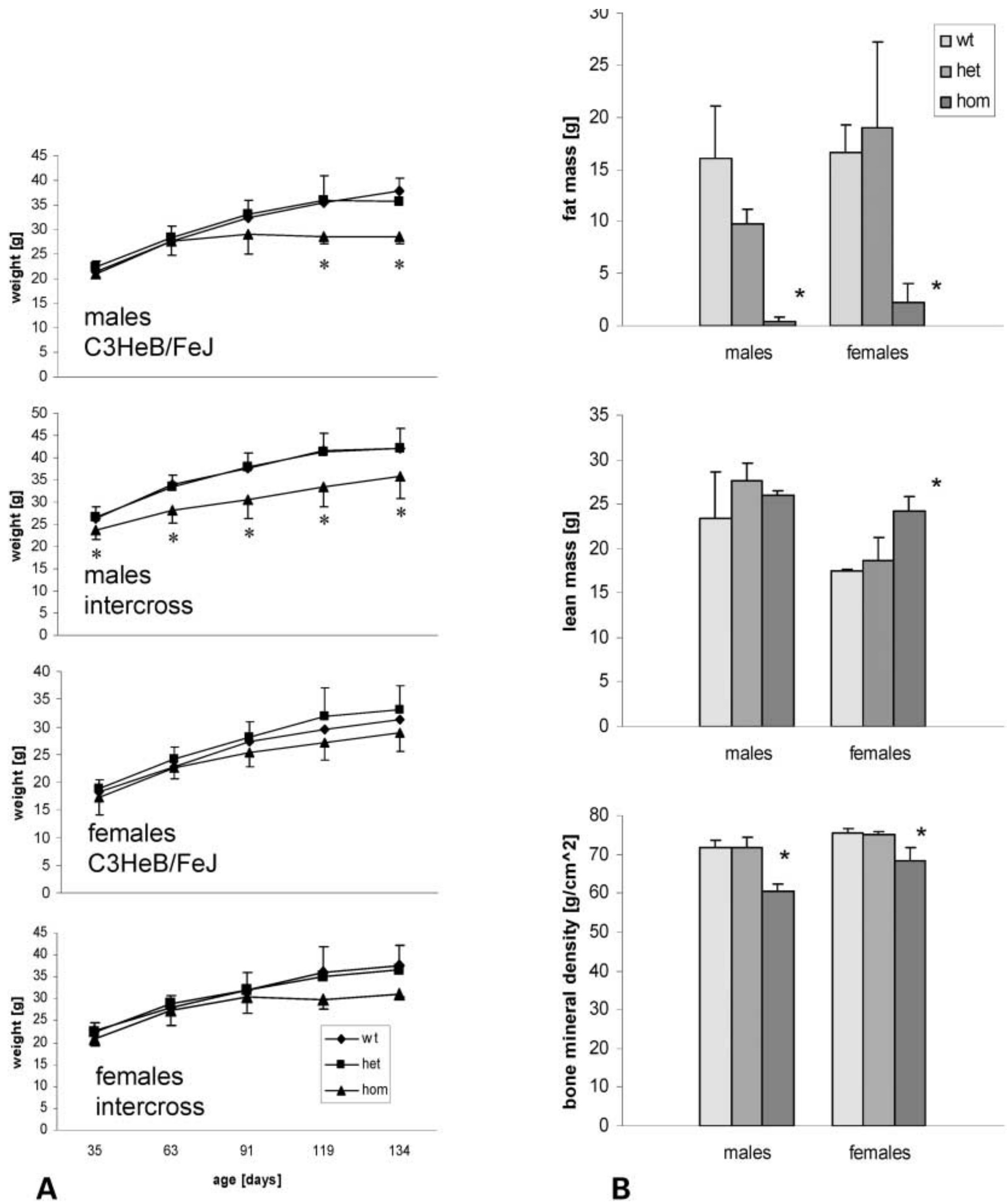

Figure 8. (**A**) Weight curves for males and females, for inbred or mixed background are represented. There is a clear difference between the development of inbred and outcross/intercross males. (**B**) Fat and lean mass and bone mineral density is represented for inbred (C3HeB/FeJ) males and females. Error bars represent 1 SD, significant differences are indicated by an asterisk; ANOVA, $P = 0.05$, Bonferroni *post hoc* test; $n \geq 4$ per genotype and date.

Expression analysis

cDNA panels representing 49 different mouse organs of both genders were screened for *Slc3a1* expression using primers 5′-GTATGTCAACGCCATGCAC-3′ (fw1) and 5′-GATGCCATT-CATGAGTCTG-3′ (rv2). The cDNAs were generated from total mouse RNA using the GibcoThermoscript RT kit by random priming with pdN6 according to the manufacturer's instructions.

For northern blot analysis 15 μg of total RNA were separated on 1.3% agarose–formaldehyde gels. The RNA was then transferred on positively charged Nylon membranes (Hybond-N+, Amersham Pharmacia) according to standard protocols. For hybridization, the probe generated with primers 5′-GATACGCTGTTGAGGATATC-3′ (fw3) and 5′-GACGGTG-TGGTAGTCAGAG-3′ (rv4) was labeled using Ambion StrizEZ Kit and hybridized overnight in UltraHyb solution (Ambion) following the manufacturer's instructions. Kidneys of homozygous *pbl/pbl* mice showed the full spectrum from no histopathological changes to severe hydronephrosis; for expression studies, we only used *pbl/pbl* kidneys without secondary changes.

LightCycler experiments were performed according to the manufacturers instructions using QuantiTect SYBR Green PCR Kit (Qiagen, Hilden). Primers for Slc3a1 were fw1 and rv4;

Downloaded from http://hmg.oxfordjournals.org/ by guest on January 13, 2014

primer sequences for the two reference transcripts acidic ribosomal phosphoprotein P0 were 5′-GGAGCAGACAACGT-GGGC-3′ and 5′-GATGTGAGGCAGCAGTTTCTC-3′ and for laminA 5′-GAGAGGAACAGCAACCTCGT-3′ and 5′-CAG-CTGCTGCTGCATCCT-3′.

Histology and *in situ* hybridization

Unless otherwise indicated, tissues were obtained from 3-month-old animals, fixed with neutral buffered 4% formaldehyde. The samples were dehydrated and embedded in paraffin. Sections of 2–4 μm thickness were produced and stained with hematoxylin and eosin (H&E) and examined and photographed with a light microscope Axioplan 2 (Zeiss).

For *in situ* hybridization, a modified standard protocol was used (40). In short, deparaffined sections were rehydrated and pretreated with proteinase K. The hybridization with the digoxigenin-labeled antisense probe in a hybridization mixture was performed at 50–53°C overnight. The digoxigenin was labeled using an ABC-kit (Vector) with the substrate Novared. Finally the sections were counterstained with hemalaun. RNA antisense probes were generated using the same primer set as for the northern blot.

Analysis of amino acid content in plasma, urine and bladder stones by mass spectrometry

Amino acids were determined in urine and plasma samples with a modified isotope-dilution method as described (41). A total volume of 3.5 μl of the respective samples was injected via liquid pumps (Series 200LC, Perkin-Elmer, USA) into an electrospray ionization (ESI) mass spectrometer (API3000, Applera, USA). Each MS/MS analysis comprised two different scan functions: neutral loss scan (NL) of 102 and multiple reaction monitoring scan (MRM). Ten complete scan cycles were monitored during data acquisition. The obtained data were processed using ChemoView (Version 1.1, Applera, USA) to calculate concentrations.

For determination of cystine in bladder stones we used the modified method as described (42). The calculi (ca. 20 μg) were dissolved in 10 ml HCl (0.2 M) before injection of 5 μl of the respective samples onto a Hypersil ODS packed column (4.6 × 100 mm, 5 μm bead size, Agilent, USA). HPLC condition consisted of the elution into the ESI-MS with a mobile phase (10% ACN, 100 mM ammonium acetate adjusted to pH 4.0 with 2 M acetic acid) at 10 min intervals and a flow rate of 200 μl/min. Q1 multiple ion scan mode (*m*/*z* 241) was used for detection of quasi-molecular ions of cystine.

Analysis of body composition

Body composition was analyzed using a pDEXA instrument (Nordland pDEXA Sabre, Stratec Medizintechnik, Pforzheim, Germany); X-rays were taken using the Faxitron Specimen Radiography System (Model MX-20, Faxitron X-ray Corporation, Wheeling, USA) according to the manufacturer's instructions. Mice were anesthetized by intraperitoneal injection of 5 μl/g body weight of 0.5% ketamin (WDT, Garbsen, Germany) and 0.2% rompun (Bayer AG, Leverkusen, Germany) in 0.9% NaCl solution.

ACKNOWLEDGEMENTS

We would like to thank Luitgard Hoher, Sebastian Kolb and Helmut Emmer for the phenotypic screen, Christiane Höhne and Susanne Stonawski for plasma and urine analysis, Petra Benhaqi for assistance in genotyping and mutation analysis, Yvonne Knack for expression profiling, Martina Weber and Wolfgang Jagla for histological staining and Anneliese Wunderlich for *in situ* hybridizations.

REFERENCES

1. Segal, S. and Thier, S.O. (1995) Cystinuria. In Scriver, C.R., Sly, W.S. and Beaudet, A.L. (eds), *The Metabolic and Molecular Bases of Inherited Diseases*, Vol. III, 7th edn. McGraw-Hill, New York, pp. 3581–3601.
2. Tate, S.S., Yan, N. and Udenfriend, S. (1992) Expression cloning of a Na(+)-independent neutral amino acid transporter from rat kidney. *Proc. Natl Acad. Sci. USA*, **89**, 1–5.
3. Bertran, J., Werner, A., Moore, M.L., Stange, G., Markovich, D., Biber, J., Testar, X., Zorzano, A., Palacin, M. and Murer, H. (1992) Expression cloning of a cDNA from rabbit kidney cortex that induces a single transport system for cystine and dibasic and neutral amino acids. *Proc. Natl Acad. Sci. USA*, **89**, 5601–5605.
4. Wells, R.G., Pajor, A.M., Kanai, Y., Turk, E., Wright, E.M. and Hediger,M.A. (1992) Cloning of a human kidney cDNA with similarity to the sodium–glucose cotransporter. *Am. J. Physiol*, **263**, F459–F465.
5. Bertran, J., Werner, A., Chillaron, J., Nunes, V., Biber, J., Testar, X., Zorzano, A., Estivill, X., Murer, H. and Palacin, M. (1993) Expression cloning of a human renal cDNA that induces high affinity transport of L-cystine shared with dibasic amino acids in *Xenopus* oocytes. *J. Biol. Chem.*, **268**, 14842–14849.
6. Lee, W.S., Wells, R.G., Sabbag, R.V., Mohandas, T.K. and Hediger, M.A. (1993) Cloning and chromosomal localization of a human kidney cDNA involved in cystine, dibasic, and neutral amino acid transport. *J. Clin. Invest*, **91**, 1959–1963.
7. Bertran, J., Magagnin, S., Werner, A., Markovich, D., Biber, J., Testar, X., Zorzano, A., Kuhn, L.C., Palacin, M. and Murer, H. (1992) Stimulation of system y(+)-like amino acid transport by the heavy chain of human 4F2 surface antigen in *Xenopus laevis* oocytes. *Proc. Natl. Acad. Sci. USA*, **89**, 5606–5610.
8. Broer, S. and Wagner, C.A. (2002) Structure-function relationships of heterodimeric amino acid transporters. *Cell Biochem. Biophys.*, **36**, 155–168.
9. Feliubadalo, L., Font, M., Purroy, J., Rousaud, F., Estivill, X., Nunes, V., Golomb, E., Centola, M., Aksentijevich, I., Kreiss, Y. *et al.* (1999) Non-type I cystinuria caused by mutations in SLC7A9, encoding a subunit (bo, +AT) of rBAT. International Cystinuria Consortium. *Nat. Genet.*, **23**, 52–57.
10. Dello Strologo L., Pras, E., Pontesilli, C., Beccia, E., Ricci-Barbini, V., de Sanctis, L., Ponzone, A., Gallucci, M., Bisceglia, L., Zelante, L. *et al.* (2002) Comparison between SLC3A1 and SLC7A9 cystinuria patients and carriers: a need for a new classification. *J. Am. Soc. Nephrol.*, **13**, 2547–2553.
11. Font, M.A., Feliubadalo, L., Estivill, X., Nunes, V., Golomb, E., Kreiss, Y., Pras, E., Bisceglia, L., d'Adamo, A.P., Zelante, L. *et al.* (2001) Functional analysis of mutations in SLC7A9, and genotype–phenotype correlation in non-Type I cystinuria. *Hum. Mol. Genet.*, **10**, 305–316.
12. Leclerc, D., Boutros, M., Suh, D., Wu, Q., Palacin, M., Ellis, J.R., Goodyer, P. and Rozen, R. (2002) SLC7A9 mutations in all three cystinuria subtypes. *Kidney Int.*, **62**, 1550–1559.
13. Schmidt, C., Albers, A., Tomiuk, J., Eggermann, K., Wagner, C., Capasso, G., Lahme, S., Hesse, A., Lang, F., Zerres, K. *et al.* (2002) Analysis of the genes SLC7A9 and SLC3A1 in unclassified cystinurics: mutation detection rates and association between variants in SLC7A9 and the disease. *Clin. Nephrol.*, **57**, 342–348.
14. Henthorn, P.S., Liu, J., Gidalevich, T., Fang, J., Casal, M.L., Patterson, D.F. and Giger, U. (2000) Canine cystinuria: polymorphism in the canine SLC3A1 gene and identification of a nonsense mutation in cystinuric Newfoundland dogs. *Hum. Genet.*, **107**, 295–303.

Downloaded from http://hmg.oxfordjournals.org/ by guest on January 13, 2014

15. Balling, R. (2001) ENU mutagenesis: analyzing gene function in mice. *Annu. Rev. Genomics Hum. Genet.*, **2**, 463–492.
16. Russ, A., Stumm, G., Augustin, M., Sedlmeier, R., Wattler, S. and Nehls, M. (2002) Random mutagenesis in the mouse as a tool in drug discovery. *Drug Discov. Today*, **7**, 1175–1183.
17. Goodyer, P., Boutros, M. and Rozen, R. (2000) The molecular basis of cystinuria: an update. *Exp. Nephrol.*, **8**, 123–127.
18. Segawa, H., Miyamoto, K., Ogura, Y., Haga, H., Morita, K., Katai, K., Tatsumi, S., Nii, T., Taketani, Y. and Takeda, E. (1997) Cloning, functional expression and dietary regulation of the mouse neutral and basic amino acid transporter (NBAT). *Biochem. J.*, **328**, 657–664.
19. Janecek, S., Svensson, B. and Henrissat, B. (1997) Domain evolution in the alpha-amylase family. *J. Mol. Evol.*, **45**, 322-–331.
20. Wells, R.G. and Hediger, M.A. (1992) Cloning of a rat kidney cDNA that stimulates dibasic and neutral amino acid transport and has sequence similarity to glucosidases. *Proc. Natl Acad. Sci. USA*, **89**, 5596–5600.
21. Fernandez, E., Carrascal, M., Rousaud, F., Abian, J., Zorzano, A., Palacin, M. and Chillaron, J. (2002) rBAT-b(0, +)AT heterodimer is the main apical reabsorption system for cystine in the kidney. *Am. J. Physiol. Renal Physiol*, **283**, F540–F548.
22. Hitotsumachi, S., Carpenter, D.A. and Russell, W.L. (1985) Dose-repetition increases the mutagenic effectiveness of *N*-ethyl-*N*-nitrosourea in mouse spermatogonia. *Proc. Natl Acad. Sci. USA*, **82**, 6619–6621.
23. Waterston, R.H., Lindblad-Toh, K., Birney, E., Rogers, J., Abril, J.F., Agarwal, P., Agarwala, R., Ainscough, R., Alexandersson, M., An, P. *et al.* (2002) Initial sequencing and comparative analysis of the mouse genome. *Nature*, **420**, 520–562.
24. Miyamoto, K., Segawa, H., Tatsumi, S., Katai, K., Yamamoto, H., Taketani, Y., Haga, H., Morita, K. and Takeda, E. (1996) Effects of truncation of the COOH-terminal region of a Na+-independent neutral and basic amino acid transporter on amino acid transport in *Xenopus* oocytes. *J. Biol. Chem.*, **271**, 16758–16763.
25. Deora, A.B., Ghosh, R.N. and Tate, S.S. (1998) Progressive C-terminal deletions of the renal cystine transporter, NBAT, reveal a novel bimodal pattern of functional expression. *J. Biol. Chem.*, **273**, 32980–32987.
26. Bovee, K.C., Bush, M., Dietz, J., Jezyk, P. and Segal, S. (1981) Cystinuria in the maned wolf of South America. *Science*, **212**, 919–920.
27. Hoppe, A., Denneberg, T., Jeppsson, J.O. and Kagedal, B. (1993) Urinary excretion of amino acids in normal and cystinuric dogs. *Br. Vet. J.*, **149**, 253–268.
28. Sahadevan, M. and Kasiske, B.L. (2002) Hyperlipidemia in kidney disease: causes and consequences. *Curr. Opin. Nephrol. Hypertens.*, **11**, 323–329.
29. Rutkowski, B., Szolkiewicz, M., Korczynska, J., Sucajtys, E., Stelmanska, E., Nieweglowski, T. and Swierczynski, J. (2003) The role of lipogenesis in the development of uremic hyperlipidemia. *Am. J. Kidney Dis.*, **41**, S84–S88.
30. Kronenberg, F., Mundle, M., Langle, M. and Neyer, U. (2003) Prevalence and progression of peripheral arterial calcifications in patients with ESRD. *Am. J. Kidney Dis.*, **41**, 140–148.
31. Block, G. and Port, F.K. (2003) Calcium phosphate metabolism and cardiovascular disease in patients with chronic kidney disease. *Semin Dial.*, **16**, 140–147.
32. Kalantar-Zadeh, K., Block, G., Humphreys, M.H. and Kopple, J.D. (2003) Reverse epidemiology of cardiovascular risk factors in maintenance dialysis patients. *Kidney Int.*, **63**, 793–808.
33. Adams, J.E. (2002) Dialysis bone disease. *Semin Dial.*, **15**, 277–289.
34. Rix, M., Andreassen, H., Eskildsen, P., Langdahl, B. and Olgaard, K. (1999) Bone mineral density and biochemical markers of bone turnover in patients with predialysis chronic renal failure. *Kidney Int.*, **56**, 1084–1093.
35. Lauderdale, D.S., Thisted, R.A., Wen, M. and Favus, M.J. (2001) Bone mineral density and fracture among prevalent kidney stone cases in the Third National Health and Nutrition Examination Survey. *J. Bone Miner. Res*, **16**, 1893–1898.
36. Abrahamsen, B., Hansen, T.B., Hogsberg, I.M., Pedersen, F.B. and Beck-Nielsen, H. (1996) Impact of hemodialysis on dual X-ray absorptiometry, bioelectrical impedance measurements, and anthropometry. *Am. J. Clin. Nutr.*, **63**, 80–86.
37. Stenver, D.I., Gotfredsen, A., Hilsted, J. and Nielsen, B. (1995) Body composition in hemodialysis patients measured by dual-energy X-ray absorptiometry. *Am. J. Nephrol.*, **15**, 105–110.
38. Woodrow, G., Oldroyd, B., Turney, J.H., Davies, P.S., Day, J.M. and Smith, M.A. (1996) Four-component model of body composition in chronic renal failure comprising dual-energy X-ray absorptiometry and measurement of total body water by deuterium oxide dilution. *Clin. Sci. (Lond.)*, **91**, 763–769.
39. Pupim, L.B., Kent, P., Caglar, K., Shyr, Y., Hakim, R.M. and Ikizler, T.A. (2002) Improvement in nutritional parameters after initiation of chronic hemodialysis. *Am. J. Kidney Dis.*, **40**, 143–151.
40. Steel, J.H., Jeffery, R.E., Longcroft, J.M., Rogers, L.A. and Poulsom, R. (1998) Comparison of isotopic and non-isotopic labelling for *in situ* hybridisation of various mRNA targets with cRNA probes. *Eur. J. Histochem.*, **42**, 143–150.
41. Chace, D.H., Hillman, S.L., Millington, D.S., Kahler, S.G., Adam, B.W. and Levy, H.L. (1996) Rapid diagnosis of homocystinuria and other hypermethioninemias from newborns' blood spots by tandem mass spectrometry. *Clin. Chem.*, **42**, 349–355.
42. Watanabe, H., Sugahara, K., Inoue, K., Fujita, Y. and Kodama, H. (1991) Liquid chromatographic-mass spectrometric analysis for screening of patients with cystinuria, and identification of cystine stone. *J. Chromatogr.*, **568**, 445–450.
43. Karolchik, D., Baertsch, R., Diekhans, M., Furey, T.S., Hinrichs, A., Lu, Y.T., Roskin, K.M., Schwartz, M., Sugnet, C.W., Thomas, D.J. *et al.* (2003) The UCSC Genome Browser Database. *Nucl. Acids Res.*, **31**, 51–54.
44. Hubbard, T., Barker, D., Birney, E., Cameron, G., Chen, Y., Clark, L., Cox, T., Cuff, J., Curwen, V., Down, T. *et al.* (2002) The Ensembl genome database project. *Nucl. Acids Res.*, **30**, 38–41.

Downloaded from http://hmg.oxfordjournals.org/ by guest on January 13, 2014